Chemical Engineering Journal 505 (2025) 159484

Contents lists available at ScienceDirect

Chemical Engineering Journal

journal homepage: www.elsevier.com/locate/cej

Nanopot plasmonic sensor platform for broad spectrum virus detection

Youngkyu Hwang [a,1], Zhi-Jun Zhao [b,1], Sangho Shin [c,d,1], Tun Naw Sut [e], Joshua A. Jackman [e], Taehoon Kim [f], Yuhyun Moon [c,g], Byeong-Kwon Ju [c,*], Jun-Ho Jeong [h,*], Nam-Joon Cho [i,*], Munho Kim [d,*]

[a] Bio-Convergence Materials Research Institute, Graduate School of Management of Technology, Hoseo University, Asan 31499, Republic of Korea
[b] Institute of Smart City and Intelligent Transportation, Southwest Jiaotong University, Chengdu 611756, PR China
[c] Department of Electrical Engineering, Korea University, Seoul 02841, Republic of Korea
[d] School of Electrical and Electronic Engineering, Nanyang Technological University, 50 Nanyang Avenue, Singapore 639798, Singapore
[e] School of Chemical Engineering and Translational Nanobioscience Research Center, Sungkyunkwan University, Suwon 16419, Republic of Korea
[f] LUCA AICell, Inc., Anyang 14055, Republic of Korea
[g] Fito Co., Ltd., Asan, 31478, Republic of Korea
[h] Department of Nano Manufacturing Technology, Korea Institute of Machinery and Materials (KIMM), Daejeon, 34103, Republic of Korea
[i] School of Materials Science and Engineering, Nanyang Technological University, 50 Nanyang Avenue, Singapore 639798, Singapore

ARTICLE INFO

Keywords:
Nanoplasmonics
Virus
Biosensors
Nanopot structures
Localized surface plasmon resonance
Colorimetric assays

ABSTRACT

Respiratory viruses have consistently posed global health threats, a fact underscored by the COVID-19 pandemic, which highlighted the urgent need for more effective screening tools. Early prevention strategies relied heavily on physical distancing due to limited knowledge about the virus and the absence of effective diagnostics, vaccines, or treatments. Although point-of-care testing (POCT) methods were eventually developed, their effectiveness is constrained by the ability of the virus to mutate, rendering these tests less reliable over time. There is a critical need for an alternative screening tool for respiratory viruses that can broadly detect virus particles and remains unaffected by viral mutations.

In here, we introduce a nanopot plasmonic sensor (NPS) platform that meets these criteria. This sensor can directly detect virus particles based on their nanoscale structural characteristics. Operating within the visible light spectrum, the NPS platform captures artificial lipid enveloped viruses (ALEVs), resulting in visually detectable color changes. These colorimetric changes and the sensor's nanoscale size-selectivity were confirmed through optical extinction measurements and simulations, which revealed the plasmonic origins of the sensor's high sensitivity. The broad detection capability and simplicity of measurement suggest that the NPS platform could serve as an effective screening tool for future pandemic preparedness.

1. Introduction

Over the last hundred years, several respiratory viruses have posed significant threats to public health, individual safety, and the global economy. Some notable outbreaks include Severe Acute Respiratory Distress Syndrome (SARS) in 2002, the swine flu outbreak (caused by the H1N1 strain) in 2009, and the Middle East Respiratory Syndrome (MERS) that emerged in 2012. A particularly impactful instance was the COVID-19 pandemic, triggered by the severe acute respiratory syndrome coronavirus 2 (SARS-CoV-2) [1]. In just three years, COVID-19 has resulted in over 400 million infections and has been responsible for over 6 million fatalities [2–5]. Sources indicate that one of the primary methods of transmission for these viruses is the inhalation of airborne droplets or aerosols produced when infected people cough or sneeze[6,7]. Additionally, touching surfaces contaminated by the virus and subsequently rubbing one's eyes, nose, or mouth can lead to infection [8]. This rapid transmission capability means that curbing the spread of such viruses early on is a key need.

At the onset of the pandemic, many nations shut their borders and instituted a range of measures termed "social distancing". These efforts included limiting large gatherings, mandating face masks [9–11], promoting air filtration [12,13], and implementing body temperature

* Corresponding authors at: Department of Electrical Engineering, Korea University, Seoul 02841, Republic of Korea (B.-K. Ju).
E-mail addresses: bkju@korea.ac.kr (B.-K. Ju), jhjeong@kimm.re.kr (J.-H. Jeong), njcho@ntu.edu.sg (N.-J. Cho), munho.kim@ntu.edu.sg (M. Kim).
[1] These authors are equally contributed.

https://doi.org/10.1016/j.cej.2025.159484
Received 30 June 2024; Received in revised form 1 November 2024; Accepted 9 January 2025
Available online 12 January 2025

checks [14] within communities [15]. These steps were taken in response to limited knowledge about the viral genetic makeup and the absence of effective diagnostics or treatments. As the pandemic progressed, there was an urgent push to develop vaccines and therapeutic drugs [16,17]. However, creating these solutions takes time, and some individuals experienced side effects like fever, vomiting, and muscle pain [18–20]. Moreover, genetic mutations of the virus can hinder diagnostic detection coverage and also reduce the efficacy of existing treatments or necessitate the creation of new vaccines and medications.

Point-of-care testing (POCT) methods using a surface acoustic wave [21], microarray [22], electrochemical sensor [23,24], and microfluidics [25,26] for detecting viruses have been developed due to rapid detection time, high efficiency, low cost, and ease for operation [27–29]. In particular, optical POCT methods based on antigen–antibody interactions [26,30,31], enzyme activation [32], aptamer [33,34], DNA [25,35], and RNA [36] binding convert the virus signal to measurable optical signals through colorimetric [25,31,37], fluorescence [36], and localized surface plasmon resonance (LSPR) techniques [30,32,38,39]. Despite their utility, these POCT methods face significant challenges for widespread public use, primarily due to their lengthy measurement times and labor-intensive processes. Furthermore, during the early stages of a pandemic, when detailed molecular-level information about viral nucleic acids and structural proteins is not yet available, it becomes particularly difficult to accurately identify infected cases. Drawing from recent pandemic experiences, it is evident that there is a critical need for the development of new technologies that can serve as interim measures until more specific interventions—such as PCR testing, rapid diagnostics, prophylactic medicines like vaccines, and treatments—are available.

Here, we demonstrate a simple and fast nanopot plasmonic sensor (NPS) to detect viruses using its size (<160 nm) that does not require processing such as labeling, antibody coating, extra electric power, or an antifouling coating [40]. Specially, captured virus particles in the nanopot induced a large change in light intensity and major peak shift based on nanoplasmonic phenomena, which also caused the platform color to change from reddish to greenish. We also examined the effects of NPS surface coverage, nanopot shape, and the size of artificial lipid enveloped viruses (ALEVs, 70 ~ 400 nm diameter) using a combination of optical extinction measurement and simulation approaches. To extend the practical feasibility of NPS, we further developed an integrated analysis package consisting of a detector and software, including user interface (UI), in order to obtain RGB values of the NPS platform as a function of ALEV concentration. The size-based detection method represents a valuable innovation, offering a quick, accessible, and cost-effective tool for early pandemic response. This is especially critical in the event of a new pandemic caused by an unknown virus.

2. Experimental section

2.1. Preparation of nanoplasmonic sensor with nanopot structure

The process began with the drop casting of UV cure resin RM-311 (Minuta Technology Co., Ltd. Korea.) on a nanohole patterned 8-inch silicon master (nanohole diameter = 200 nm, depth = 100 nm, pitch = 340 nm), which is prepared using electron beam lithography (e-beam) combined with KrF(248 nm laser wavelength) photolithography. After placing PET film on the resin, UV curing was performed for 90 s and then 1st replica was detached from a silicon master. The molding process was repeated to form final stamp which is same as an original pattern of a silicon master without pattern distortion [41]. Next, Au with 10 nm thickness was deposited on the stamp using e-beam evaporation (Daeki Hi-Tech Co., Ltd., Korea) at a deposition rate of 1.0 ~ 1.2 Å/s under a high-vacuum state of ~10^{-6} Torr, and then nano-hole metal layer was transferred to the target PET substrate by pressing at 160 ℃ and 6 bars for 10 min. (Supporting information S1). Etching process using Asher equipment (gas = O_2, flow = 50 s.c.c.m., power = 50 W ~ 200 W, Femto Science, Korea) generated nanopot structure due to the isotropic etching [42].

2.2. Characterization of nanoplasmonic sensor

The sample images were obtained using SEM (S-4700, Japan) and focused ion beam (FIB, Thermofisher, USA). AFM images and surface roughness of PS and NPS were obtained using an NX-10 instrument (non-contact mode, scan area = 1 μm × 1 μm, scan rate = 0.6 Hz, Park Systems, Suwon, Republic of Korea) with a cantilever (AC160TS, force constant of ≈26 N/m, Olympus, Germany). Optical extinction spectra of PS and NPS were measured using a microplate reader (SpectraMax iD5, Molecular Devices, San Jose, CA, USA). Bulk refractive index sensitivity was measured by incubating PS and NPS in water–glycerol mixtures with increasing glycerol fractions (0–40 % v/v). For practical test, artificial saliva (SAE0149, Sigma-Aldrich, St. Louis, MO, USA) was used directly to the sample and bovine serum albumin (BSA) protein (MilliporeSigma, Burlington, MA, USA) were prepared in 10 mM Tris buffer (150 mM NaCl, pH 7.5). 1,2-dioleoyl-*sn*-glycero-3-phosphocholine (DOPC) lipids dissolved in chloroform were acquired from Avanti Polar Lipids (Alabaster, AL, USA). Vesicles were prepared by the extrusion method, as previously described [43]. Aliquot of DOPC chloroform solution containing 5 mg lipid was added into a glass vial and dried with nitrogen gas to form a dry lipid film on the wall. Then, the vial was stored in a vacuum chamber overnight to remove chloroform residues. Next, 1 mL of Tris buffer (10 mM Tris, 150 mM NaCl, pH 7.5) was added to hydrate the lipid film to 5 mg/mL and the lipid suspension was vortexed for 3 min. Afterwards, the vesicles were extruded with a 100-nm polycarbonate filter by passing the lipid suspension through a Mini-Extruder (Avanti Polar Lipids) for a total of 11 times. The size distribution of extruded vesicles was determined by dynamic light scattering experiments using an ELSZ-2000 instrument (Otsuka Electronics Co., Ltd, Osaka, Japan), as previously described [44]. The average intensity-weighted vesicle size was measured to be around 125 nm. Before the experiments, the vesicles were diluted in Tris buffer to 0.2 mg/mL. For visualization test, NPS was incubated with 0.3 mg/mL virus-like particle solution for 4 h followed by extensive rinsing with MilliQtreated water. After vesicle treatment was complete, the samples were incubated in a 2 % v/v aqueous glutaraldehyde solution, followed by water rinsing. The samples were extensively dried, and then coated with a 10 nm thick layer of gold with a JFC-1600 sputter coater (Auto Fine Coater, JEOL, Tokyo, Japan) (20 mA, 60 sec). SEM imaging was performed using a FESEM 7600F instrument (JEOL, Japan) with an acceleration voltage of 5 kV at different magnifications.

2.3. Finite-Difference Time-Domain (FDTD) simulation of nanoplasmonic sensor

To perform the simulation, we set gold membrane (thickness = 30 nm) and PET film (thickness = 100 μm) and perfectly matched layer (PML) techniques was used to improve the efficiency of modeling calculation for the nanohole array. The plane wave source used at this work was a frequency of 524.637 THz with a pulse length (fs) of 2.65788, an offset (fs) of 7.53596, and a bandwidth of 449.689. The n and k values of ALEV were extracted with Ellipsometry (Supporting information S2).

2.4. Color analysis

The virus detection machine was composed of four main parts; a standard illumination source, a camera, a rectangle frame, and software. The dimensions of the frame were 16 cm × 20 cm × 24 cm (L × W × H) and it had black color blanket to block the incidence light from outside. For an illumination system, a LED light (FTS-B-100X100-HSW, Trivision, South Korea) and a digital 8 bit controller (FTS1-2250 M, Trivision, South Korea) were placed on the bottom of frame. The camera

(resolution = 1920 × 1080, Razer Kiyo Pro, Razor, Irvine, CA, USA) was located on the top of the frame with distance controller. UI and driving software were developed through Microsoft Foundation Class (MFC) programming to analyze the visible region color of the plasmonic biosensor. Standard RGB data from bare and ALEV treated sample images was collected and then the dark background and white hole in total pixels of the film were excluded. The selected pixels were used to calculate the average of the red, green, and blue values, respectively.

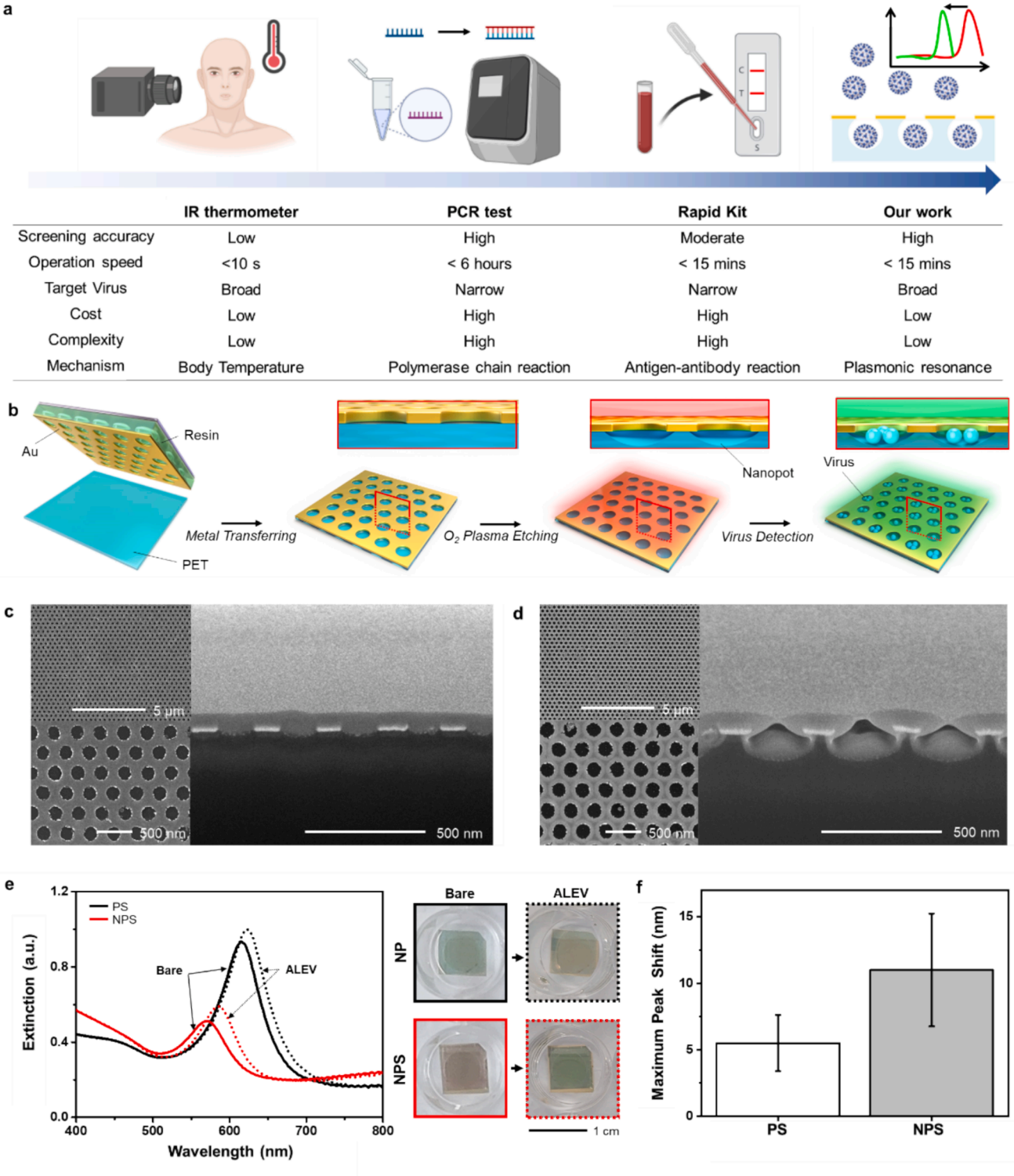

	IR thermometer	PCR test	Rapid Kit	Our work
Screening accuracy	Low	High	Moderate	High
Operation speed	<10 s	< 6 hours	< 15 mins	< 15 mins
Target Virus	Broad	Narrow	Narrow	Broad
Cost	Low	High	High	Low
Complexity	Low	High	High	Low
Mechanism	Body Temperature	Polymerase chain reaction	Antigen-antibody reaction	Plasmonic resonance

Fig. 1. Nanoplasmonic sensor based on nanopot structure (NPS) for virus detection. (a) Comparison of conventional virus detection methods (IR temperature sensor, PCR, rapid antigen kit) and our work. (b) Schematic of fabrication steps and operating principle of NPS. (c,d) SEM images of PS and NPS (Au mesh thickness = 28 nm, nanohole diameter = 200 nm, pitch = 340 nm, depth = 100 nm). (e) Optical extinction spectra of PS and NPS before and after incubation with Artificial Lipid Enveloped Virus (ALEV) containing solution at room temperature for 15 min. The red and black line with solid and dot in Fig. 1e correspond to photographs of PS and NPS before and after incubation with ALEV contained solution. (f) Summary of maximum peak shift before and after ALEV incubation (n = 3).

3. Results and discussion

3.1. Preparation of NPS

Fig. 1a presents a comparison of conventional methods, including infrared (IR) thermometer, polymerase chain reaction (PCR) test, and rapid antigen kits and the technology developed in this work, to detect virus-infected individuals. The IR temperature sensor is widely used for mass screening at airports, border crossings, and seaports during pandemics due to simplicity, rapid response, low cost, and non-physical contact, but it has low accuracy by environmental conditions such as distance, angle, and humidity [14]. PCR testing is the most accurate technique to detect viruses directly using viral genetic materials enclosed within the lipid envelope [28]. In general, it requires relatively longer time (one hour to a couple of days) to obtain results due to complex sample processing that depends on PCR type, primer, and probe. In the case of Rapid Kit, we consider two perspectives, 1) Preparation of POCT and 2) Simplicity of analysis process. That require lots of time to discover genetic information of unknown virus and to develop target antibody against virus. In the analysis process, sample collection (e.g. swabbing method) from patient or infected people needs accessories (cotton, gauze) and also causes pain by touching sensitive and weak surfaces. It requires cell lysis step and reaction time for antigen–antibody binding to produce color change [45]. Of note, PCR tests and rapid antigen kits require genetic information about the virus strain to design the primer or antibody. Compared to commercial methods, our work demonstrates that NPS can directly detect the virus itself without requiring additional processes such as cell lysis, DNA labelling, or antigen–antibody binding interactions. This technology can lead to a new virus collection method (e.g. breath analyzer) without complicated and painful process [46].

Fig. 1b shows the fabrication and operating principles of the NPS platform for virus detection. Briefly, after Au deposition on the template with nanohole array, the Au nanohole array was transferred onto a polyethylene terephthalate (PET) film using nanotransfer, which does not require additional glue layer (See the details for the preparation of the template in Supporting Information S1) [47].

Next, O_2 plasma etching process forms the nano-scale cavity (nanopot) with 100 nm of depth and 250 nm of diameter underneath the Au nanomembrane, which is bigger than typical virus size (~160 nm) (Fig. 1c). To identify the role of nanopot, we compared NPS to plasmonic sensor (PS), which is a sample before O_2 plasma etching in this study. After etching process, the surface of the nanopot and Au nanomembrane showed an increase in surface roughness, but there was no noticeable distortion and thickness change of the Au nano patterns (Supporting Information S3). The nanopot structure generates a change in the optical spectrum such as position, extinction, and shape of peak in the visible light range. For example, NPS showed a blueshift of the maximum peak from 615 nm to 571 nm, and also a color change from blue to red (Fig. 1e). The blueshift can occur due to the change in effective refractive index of the environment [32,39].

To characterize sensing capabilities, we measured bulk sensitivity, which is an important criterion to evaluate the performance of nanoplasmonic sensors [48]. NPS showed slightly improved bulk sensitivity of 163 nm/RIU compared to plasmonic sensor (PS, 123 nm/RIU) (Supporting Information S4). Furthermore, since most virus pandemics are caused by membrane-enveloped viruses, we prepared 1,2-dioleoyl-*sn*-glycero-3-phosphocholine (DOPC) lipid vesicles as an artificial lipid enveloped virus (ALEV) using the extrusion method and compared the maximum peak position of the PS and NPS after ALEV coating (See the details in Experimental Section) [49]. After ALEV incubation for 15 mins, the NPS platform showed a large maximum peak shift of 11.0 ± 4.2 nm and noticeable color change from red to green as compared to the value of 5.5 ± 2.1 nm and neglectable color change for the PS platform (Fig. 1f). We also tested nanoplasmonic sensors with various diameters, pitches, and thicknesses of the Au nanohole patterns (diameter: 170 ~ 230 nm, pitch: 340 ~ 500 nm, thickness: 28 ~ 80 nm) (Supporting Information S5-S9). Although all samples after O_2 plasma treatment showed 2 times higher maximum peak shifts than those of the bare samples after ALEV coating, only Au nanohole pattern with 200 nm of a diameter, 340 nm of a pitch, and 28 nm of Au thickness exhibited a remarkable color change from red to green, which can be distinguished even by the naked eye (Supporting Information S10-S12). The shape of the nanopot structure also can affect the sensitivity of NPS, for example, the optimized size of nanopot which can contain 2 ~ 3 ALEVs showed the most effective sensitivity to generate a visible color change.

3.2. Origin of the plasmonic enhancement effect

We performed finite-difference time-domain (FDTD) simulations to investigate the origin of the plasmonic enhancement effect based on the nanopot geometrical specifics and ALEV capture (Fig. 2). To improve accuracy, the design of the PS, NPS, and ALEV-captured NPS structures for optical simulation were based on the geometrical and optical information of actual samples, including diameter, height, and width of nanopots and the refractive index (n) and extinction coefficient (k) of ALEVs (Fig. 2d-f, Supporting Information Fig. S1 and S13). In the case of PS, the light intensity at the edge of the Au nanomembrane that faced the PET film was relatively strong compared to other regions (underneath of Au nanofilm) due to the short-range distribution of the electric field (Fig. 2g and 2 h). After nanopot formation, the simulation result showed 1.5 times higher light intensity at the edge of the Au nanomembrane than that of PS due to the combination of the increase in exposed surface area of the Au nanomembrane and the nanopores that are smaller than the light wavelength, while the real optical spectrum of NPS showed a decrease in the peak intensity. It is possible that the non-rectangular shape of the Au edge and the relatively high surface roughness of the Au nanomembrane and PET might contribute to the decrease in light intensity [50]. In addition, the light intensity of the NPS platform increased by up to ~ 1.6 times at the edge of the Au nanomembrane depending the number of captured ALEV (Fig. 2i). The peak shift due to ALEV capture was induced by the change in the external dielectric environment and hence refractive index shift increase from air to ALEV, which resulted in the experimentally observed maximum peak shift increase [51,52]. Of note, the captured ALEV that exhibits a nanoscale spherical shape also generated noticeable light intensity between the edge of Au nanomembrane and ALEV, which could contribute to the additional increase in peak intensity. As the number of ALEVs in the nanopot increased from 0 to 3, there was also additional gradient enhancement of the light intensity at the top and in the middle of the nanopot (Supporting Information Fig. S14). This result indicated that the combination of the nanopot and ALEV mainly affected the peak intensity and the magnitude of the maximum peak shift, which resulted in a large color change for virus detection. In addition, the repetition of ALEV coating process and the high concentration of ALEV can produce the significant color changes visible to bare eyes by increasing the number of ALEV in nanopot.

3.3. Optical characterization of the NPS

To clarify the origin of the color change, we measured the maximum peak shift of NPS using ALEVs with various diameters (70 nm, 100 nm, and 400 nm) (Fig. 3a and Supporting Information S15). In the case of 400 nm ALEV, which is bigger than the diameter of the Au nanohole, it induced only a 2.6 ± 1.5 nm redshift in the maximum peak position. However, ALEVs with 70 nm and 100 nm diameters that are smaller than the Au nanohole yielded 17.3 ± 0.6 nm and 14.3 ± 0.6 nm maximum peak shifts, respectively. To visualize the size-dependent capture of ALEV, we placed NPS in DI water containing polystyrene beads with diameters of 100 nm and 400 nm for 15 mins. After washing, there was no 400 nm diameter bead in nanopot structure, but various numbers of 100 nm diameter beads were observed inside nanopot

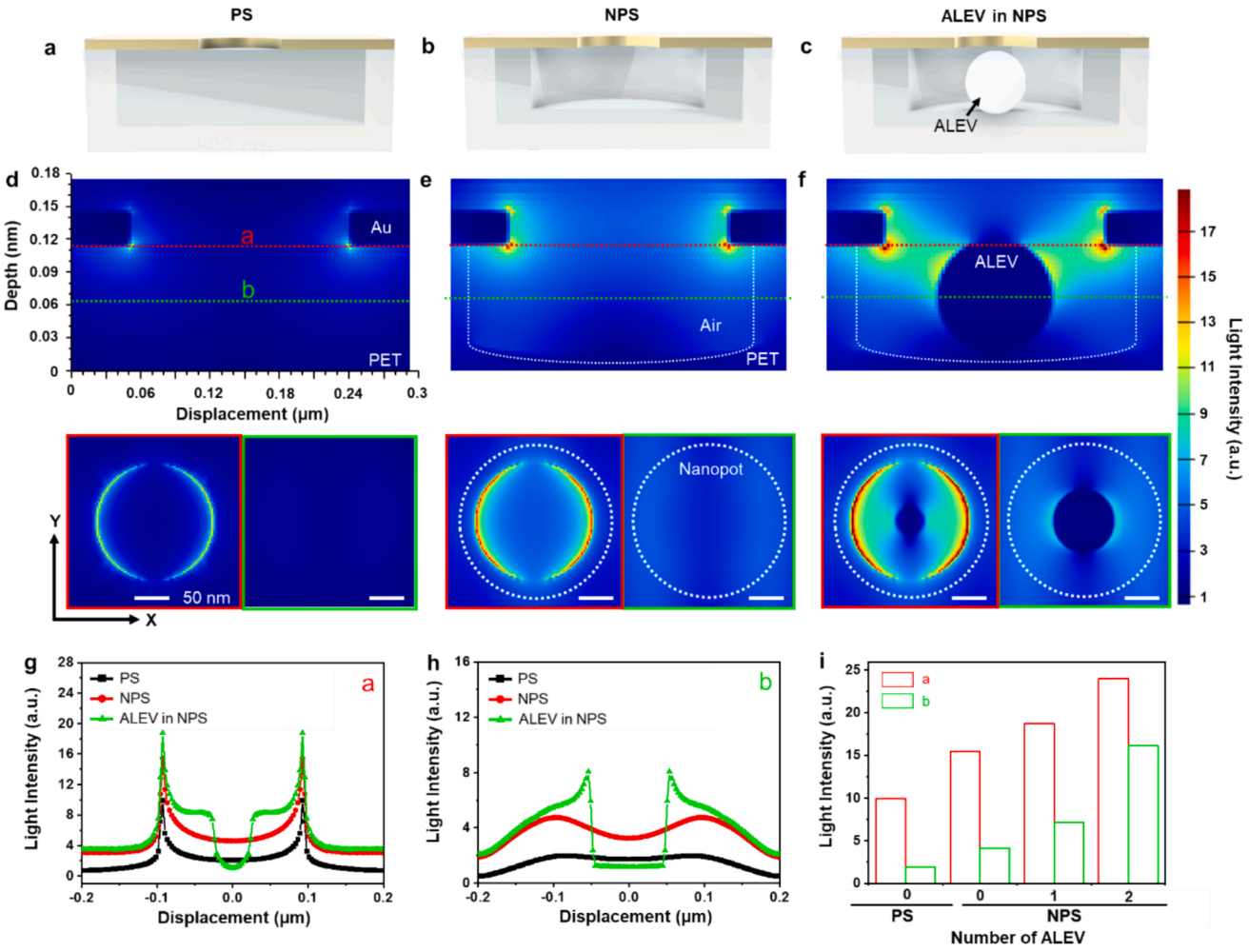

Fig. 2. FDTD simulations for modeling plasmonic effect of NPS platform to detect virus particles. (a-c) Schematic of nanoplasmonic sensor structures for FDTD simulation: (a) bare (PS), (b) O_2 plasma treated (NPS), and (c) virus captured conditions (Captured ALEV in NPS). (d-f) Cross-sectional image of simulated light intensity of nanoplasmonic sensor. Red and green boxes represent top view of the plane cut along the red (a) and green (b) dotted line. (g-h) Light intensity of nanoplasmonic sensors corresponding to the red (a) and green (b) dotted line. (i) Comparison of plasmonic effect depending on the formation of nanopot structure and the number of ALEVs in a nanopot.

structures (Supporting Information S16). Importantly, nanobeads showed color change. This means that the samples containing nanoparticles with similar shape and size can produce false positive. To overcome this issue, further research is needed to determine what the kind of the nanoparticles are contained in saliva and breath. We also used the lipid vesicles to visualize how ALEVs are captured in the nanopots (Supporting Information S17). These results support that an optimized nanohole diameter provides virus selectivity through size-dependent control via a steric effect. To validate that the nanopot is the key platform component contributing to the sensing detection, we coated Au nanomembranes of PS and NPS with thiol-terminated methoxy polyethylene(glycol) (mPEG-SH), which binds to the Au surface only. Although NPS showed a slightly higher maximum peak shift (4.5 ± 3.5 nm) than that of PS (3.0 ± 2.6 nm) due to the increase in the surface area by the undercut etching, the difference between PS and NPS is neglectable (Fig. 3b). This finding supports that the nanopot formed in the PET film mainly contributes to the maximum peak shift rather than binding to the Au surface.

Next, we evaluated the effects of adding Tris buffer, artificial saliva, bovine serum albumin protein (BSA, dimensions = ~14 nm × 4 nm × 4 nm), or ALEVs to the NPS platform because biological specimens used for screening often contain various foreign materials such as volatile organic compounds (VOCs), exosome, and proteins in addition to viruses (Fig. 3c and Supporting Information S18). Among the various conditions, the ALEV coating induced the largest redshift in the maximum peak with 12 ± 0.6 nm, while Tris buffer, artificial saliva, and BSA showed -5.0 ± 0.6 nm, -8.3 ± 0.7 nm, and 0.3 ± 0.7 nm shifts, respectively. Interestingly, BSA with 10 μM and 125 μM of concentration showed similar redshift in the maximum peak. This result indicates that small size (less than 7 nm) of particles could be minor effect on red shift of peak. To measure the sensitivity of the nanoplasmonic sensor, we tested various ALEV concentrations (i.e., 1.25, 12.5, 125, and 250 μM) (Fig. 3d, Supporting Information S19 and S20). As the concentration increased, the nanoplasmonic sensors showed a gradual increase in the maximum peak shift from -6.3 ± 0.8 nm to 11.6 ± 1.3 nm. In addition, we repeated the coating process, which involved incubating the sample for 15 mins followed by washing 3 times with deionized water, up to 5 times with Tris-buffer, artificial saliva, BSA (10 μM), and ALEV (125 μM). All cases exhibited saturation after 2- or 3-times application of the coating process and, in the case of the ALEV coating, it showed the largest maximum peak shift (21.3 ± 2.9 nm) and greenish color (Fig. 3e, Supporting Information S21 and S22).

3.4. Colorimetric analysis using optical detection setup

To detect viruses in a systematic way, we developed an optical detection setup, including an image capturing part (i.e., sample holder, light source, power supply, and detector) and a processing part (i.e., a

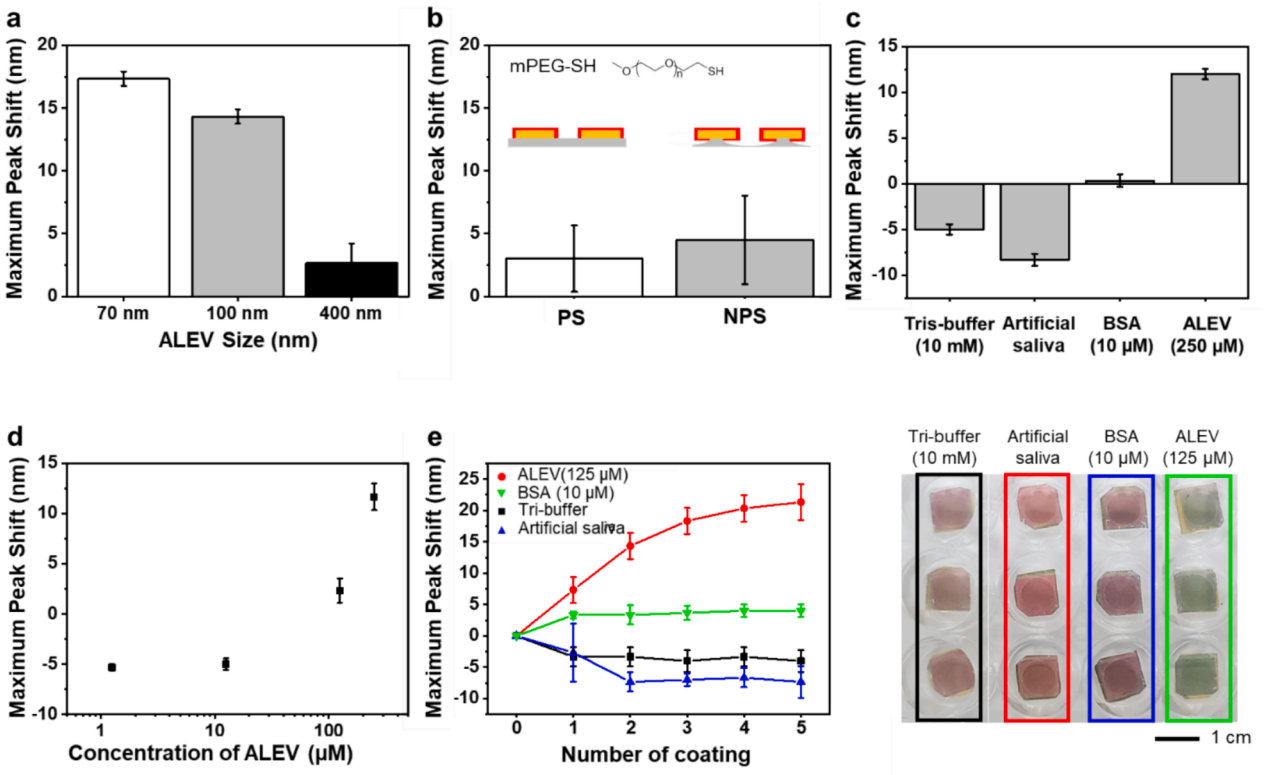

Fig. 3. Optical characterization of the NPS platform. (a) Maximum peak shift of NPS as a function of ALEV size (n = 3). (b) Nanoplasmonic effect of PS and NPS to ALEV after coating with mPEG-SH (n = 3). (c) Maximum peak shift of NPS under various conditions: Tris buffer, artificial saliva, BSA, and ALEV (n = 3). (d) NPS response to increasing ALEV concentration (1.25 ~ 250 μM, n = 3). (e) Maximum peak shift of NPS (dimension = 0.9 mm × 0.9 mm) as a function of the number of coating steps using ALEVs (red), BSA (green), Tris-buffer (black), and artificial saliva (blue). Red, green, black, and blue lines correspond to photographs of NPS in each color box.

color analysis software) (Supporting Information S23). Fig. 4a shows an illustration of the virus detection process and the corresponding change in optical extinction spectrum. To avoid color distortion caused by light reflection, the light source (10 cm × 10 cm) was placed at the NPS backside (1 cm × 1 cm) and the detector captured transmitted light only in dark condition. As a first step, we obtained a bare NPS image from the detector and extracted color information according to the RGB color scale (0 ~ 255), which are three primary colors of light. RGB value means 256 levels of brightness from black (0, minimum light intensity) to white (255, maximum light intensity). We selected the pixels in each color value range of red (150 ~ 255), green (120 ~ 220), and blue (150 ~ 255) from a total of 307,200 pixels in a single NPS image to minimize noise. For example, the number of each color value range (0 ~ 149, 0 ~ 119) means a sample holder part in the images that can affect the real signals, and hence can be excluded.

Next, different ALEV concentrations (0 ~ 500 μM) were applied to the NPS platform for 15 mins and washed with DI water thrice. After ALEV-coated NPS images were obtained, we calculated color change compared to the NPS platform without ALEV (Fig. 4b). As the ALEV concentration increased, the blue color showed no noticeable trend whereas the green color exhibited a gradual increase in the color change but was still relatively small ($-4.0 \pm 4.0 \sim 5.7 \pm 0.7$). However, the red color showed a dramatic increase in the color change from -6.0 ± 4.1 to 32.8 ± 14.2 as a function of ALEV concentration. Pixel distribution of red color before and after ALEV coating clearly showed a separated pixel distribution (Fig. 4c-e). By contrast, the pixel distribution of green and blue colors before and after ALEV coating was overlapped (Fig. 4f-k). This result indicates that the red color is the most critical value to analyze for virus detection using NPS compared to green and blue colors. We also tested NPS using real virus samples from covid-19 patients (data is not shown). It showed that the sensitivity and specificity of NPS are 93.8 % and 57.1 %, respectively (Cut-off value of color change = 8).

4. Conclusion

We have developed a systematic approach to detect viruses based on a NPS platform. The buried nanopot structure is intentionally formed in the nanohole area of Au nanomembranes on PET films and captures the virus using its size only. Importantly, the significant change in peak position of extinction spectra resulted from the captured virus and induces a visible color change that can be analyzed by the optical detection setup. While other approaches that have demonstrated the high selectivity using the molecular features of viruses such as viral proteins or nucleic acids could be inactivated by genetic mutations, a unique feature of the NPS in our work provides a long-term stability because it is based on the size of viruses and additional processes such as labeling, antibody coating, extra electrical power, or antifouling coating are not required. In summary, our method can help to realize high accuracy and fast speed virus detection via a simple and low-cost process and NPS platforms could therefore lead to a new class of screening technologies for broad spectrum virus detection in public spaces.

CRediT authorship contribution statement

Youngkyu Hwang: Writing – original draft, Methodology, Conceptualization. **Zhi-Jun Zhao:** Methodology. **Sangho Shin:** Writing – original draft, Methodology. **Tun Naw Sut:** Methodology. **Joshua A. Jackman:** Writing – review & editing. **Taehoon Kim:** Software. **Yuhyun Moon:** Software. **Byeong-Kwon Ju:** Writing – review & editing. **Jun-Ho Jeong:** Writing – review & editing. **Nam-Joon Cho:** Writing – review & editing, Project administration. **Munho Kim:** Writing – review & editing, Supervision.

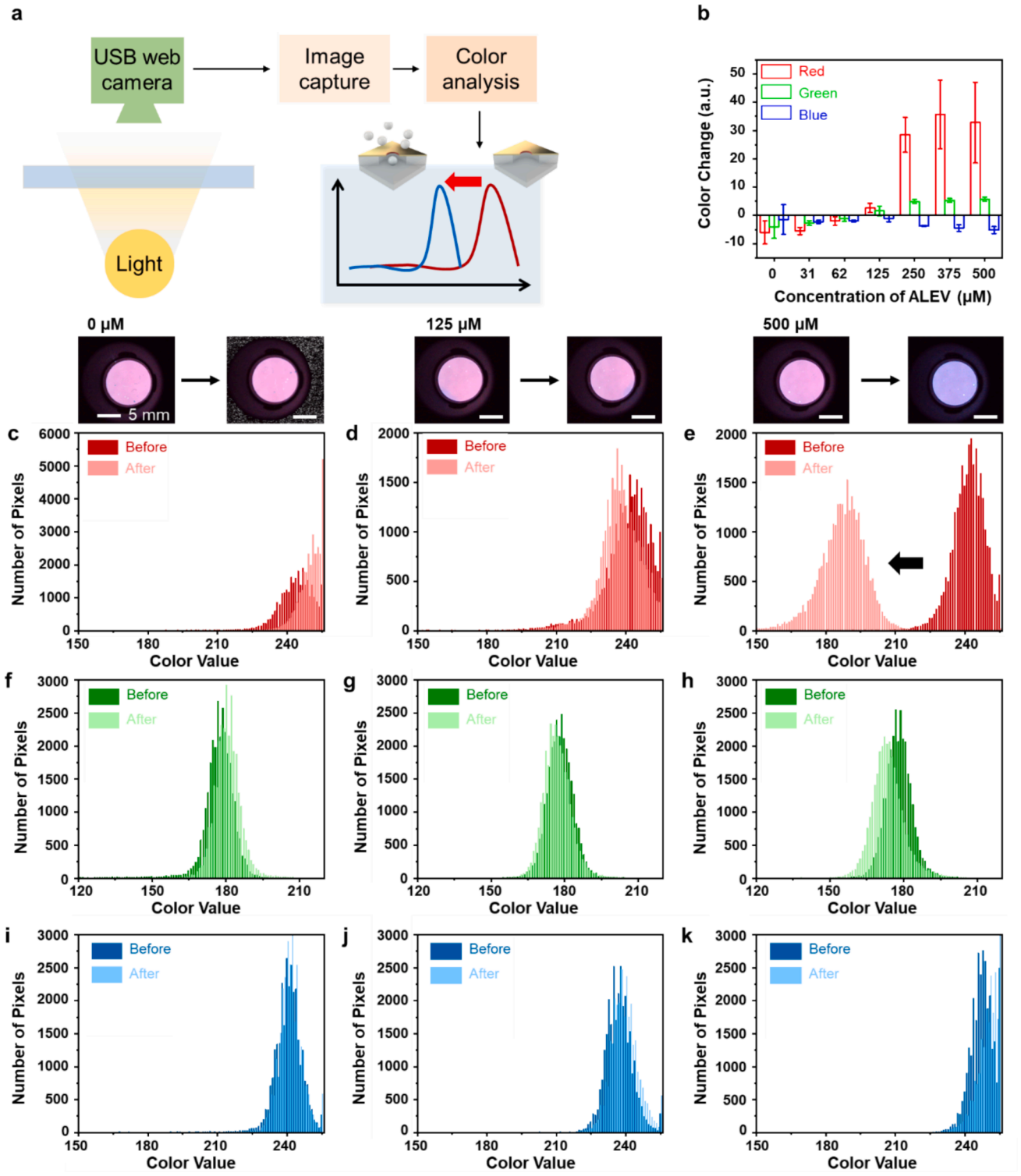

Fig. 4. Colorimetric analysis for virus detection using NPS. (a) Illustration shows measurement process overview, including color detection, image capture, data analysis steps, and principle of color change. (b) Summary of relative color change of NPS according to red, green, and blue color channels before and after incubation with various ALEV concentrations. (c-k) Representative graphs show the pixel distribution as a function of color value in the range of 0 ~ 255 after incubation in ALEV-containing solution with various ALEV concentrations (0 μM, 125 μM, and 500 μM).

Declaration of competing interest

The authors declare that they have no known competing financial interests or personal relationships that could have appeared to influence the work reported in this paper.

Acknowledgment

This work was supported by Ministry of Education, Singapore, under the Grant ACRF Tier 1 grant (RG129/22). This work was also supported by the Basic Science Research Program through the National Research Foundation of Korea (NRF) funded by the Ministry of Education

(2021R1I1A1A01056302 and RS-2023-00246169) and the NRF grant funded by the Korean government (MSIT) (2020R1C1C1004385, 2020R1C1C1013567, and 2022M3H4A1A04096380). This work was also partially supported by the SKKU Global Research Platform Research Fund, Sungkyunkwan University, 2023. In addition, this work was supported by a Ministry of Culture, Sports and Tourism and Korea Creative Content Agency (R2022020033), and the Development Program of Machinery and Equipment Industrial Technology (20018235, Development of inline nano-imprinter for nano photonic device funded by the Ministry of Trade, industry & Energy (MI, Korea). The Technology Innovation Program (No. 20019400) funded by the Ministry of Trade, Industry & Energy (MOTIE, Korea), the Brain Korea 21 Project in 2024, and the National Natural Science Foundation of China under Grant 52375578 supported this work. This work was partly supported by the Institute of Information & Communications Technology Planning & Evaluation(IITP)-Innovative Human Resource Development for Local Intellectualization program grant funded by the Korea government (MSIT)(RS-2024-00436765) and Alchemist Project grant funded by Korea Evaluation Institute of Industrial Technology (KEIT) & the Korea Government (MOTIE) (Project Number: 1415179744, 20019169).

Appendix A. Supplementary data

Supplementary data to this article can be found online at https://doi.org/10.1016/j.cej.2025.159484.

Data availability

Data will be made available on request.

References

[1] S. Tomczyk, A. Taylor, A. Brown, M.E.A. de Kraker, A. El-Saed, M. Alshamrani, R. S. Hendriksen, M. Jacob, S. Lofmark, O. Perovic, N. Shetty, D. Sievert, R. Smith, J. Stelling, S. Thakur, A.C. Vietor, T. Eckmanns, Impact of the COVID-19 pandemic on the surveillance, prevention and control of antimicrobial resistance: a global survey, J. Antimicrob. Chemother. 76 (11) (2021) 3045–3058, https://doi.org/10.1093/jac/dkab300.

[2] E.J. Chow, T.M. Uyeki, H.Y. Chu, The effects of the COVID-19 pandemic on community respiratory virus activity, Nat. Rev. Microbiol. 21 (3) (2023) 195–210, https://doi.org/10.1038/s41579-022-00807-9.

[3] W. Msemburi, A. Karlinsky, V. Knutson, S. Aleshin-Guendel, S. Chatterji, J. Wakefield, The WHO estimates of excess mortality associated with the COVID-19 pandemic, Nature 613 (7942) (2023) 130–137, https://doi.org/10.1038/s41586-022-05522-2.

[4] M. Zarei, D. Bose, M. Nouri-Vaskeh, V. Tajiknia, R. Zand, M. Ghasemi, Long-term side effects and lingering symptoms post COVID-19 recovery, Rev. Med. Virol. 32 (3) (2022) e2289.

[5] WHO. WHO Coronavirus (COVID-19) Dashboard (2021).

[6] M.A. Kohanski, L.J. Lo, M.S. Waring, Review of indoor aerosol generation, transport, and control in the context of COVID-19, Int. Forum Allergy Rhinol. 10 (10) (2020) 1173–1179, https://doi.org/10.1002/alr.22661.

[7] C.C. Wang, K.A. Prather, J. Sznitman, J.L. Jimenez, S.S. Lakdawala, Z. Tufekci, L. C. Marr, Airborne transmission of respiratory viruses, Science 373 (6558) (2021) eabd9149, https://doi.org/10.1126/science.abd914.

[8] N. Wang, A.R. Ferhan, B.K. Yoon, J.A. Jackman, N.-J. Cho, T. Majima, Chemical design principles of next-generation antiviral surface coatings, Chem. Soc. Rev. 50 (17) (2021) 9741–9765, https://doi.org/10.1039/D1CS00317H.

[9] R.A. Bataglioli, J.B.M.R. Neto, G.B. Calais, L.M. Lopes, J. Tsukamoto, A.P. de Moraes, C.W. Arns, M.M. Beppu, Hybrid alginate-copper sulfate textile coating for coronavirus inactivation, J. Amer. Ceramic Soc. 105 (3) (2022) 1748–1752, https://doi.org/10.1111/jace.17862.

[10] S. Currie, T. Cutts, S. Kasloff, W. Wang, K. Holloway, S. Logsetty, A. Kumar, A. Kumar, S. Liu, Rechargeable Potent Anti-Viral Cotton Grafted with a New Quaternized N-Chloramine, Adv. Mater. Interfaces 9 (35) (2022) 2201338, https://doi.org/10.1002/admi.202201338.

[11] W. Shao, J. Li, Y. Zhang, N. Sun, T. Wu, M. Yan, F. Liu, H. Jiang, X. Chen, J. He, Polyvinylidene fluoride multi-scale nanofibrous membrane modified using N-halamine with high filtration efficiency and durable antibacterial properties for air filtration, J. Colloid Interface Sci. 628 (Pt B) (2022) 627–636, https://doi.org/10.1016/j.jcis.2022.08.077.

[12] F. Soto, M.O. Ozen, C.F. Guimaraes, J. Wang, K. Hokanson, R. Ahmed, R.L. Reis, R. Paulmurugan, U. Demirci, Wearable Collector for Noninvasive Sampling of SARS-CoV-2 from Exhaled Breath for Rapid Detection, ACS Appl. Mater. Interfaces 13 (35) (2021) 41445–41453, https://doi.org/10.1021/acsami.1c09309.

[13] H. Kim, S.K. Hong, H. Lee, Y. Jeong, S.J. Cho, A reusable nanofibrous air filter with anti-wetting microbead coating, J. Clean. Prod. 382 (2023) 134972, https://doi.org/10.1016/j.jclepro.2022.134972.

[14] J.F. Spindel, S. Pokrywa, N. Elder, C. Smith, The environment has effects on infrared temperature screening for COVID-19 infection, Am. J. Infect. Control 49 (11) (2021) 1445–1447, https://doi.org/10.1016/j.ajic.2021.08.002.

[15] L. Pan, J. Wang, X. Wang, J.S. Ji, D. Ye, J. Shen, L. Li, H. Liu, L. Zhang, X. Shi, L. Wang, Prevention and control of coronavirus disease 2019 (COVID-19) in public places, Environ. Pollut. 292 (Pt B) (2022) 118273, https://doi.org/10.1016/j.envpol.2021.118273.

[16] J. Zhao, S. Zhao, J. Ou, J. Zhang, W. Lan, W. Guan, X. Wu, Y. Yan, W. Zhao, J. Wu, J. Chodosh, Q. Zhang, COVID-19: Coronavirus Vaccine Development Updates, Front Immunol. 11 (2020) 602256, https://doi.org/10.3389/fimmu.2020.602256.

[17] C. Stasi, S. Fallani, F. Voller, C. Silvestri, Treatment for COVID-19: An overview, Eur J Pharmacol. 889 (2020) 173644, https://doi.org/10.1016/j.ejphar.2020.173644.

[18] A. Pormohammad, M. Zarei, S. Ghorbani, M. Mohammadi, M. H. Razizadeh, D. L. Turner, R. J. Turner, Efficacy and Safety of COVID-19 Vaccines: A Systematic Review and Meta-Analysis of Randomized Clinical Trials, Vaccines (Basel) 9 (5) (2021) 467, https://doi.org/10.3390/vaccines9050467.

[19] Y.D. Li, W.Y. Chi, J.H. Su, L. Ferrall, C.F. Hung, T.C. Wu, Coronavirus vaccine development: from SARS and MERS to COVID-19, J. Biomed. Sci. 27 (1) (2020) 104, https://doi.org/10.1186/s12929-020-00695-2.

[20] I. Aygun, M. Kaya, R. Alhajj, Identifying side effects of commonly used drugs in the treatment of Covid 19, Sci. Rep. 10 (1) (2020) 21508, https://doi.org/10.1038/s41598-020-78697-1.

[21] W. Lee, J. Jung, Y. K. Hahn, S. K. Kim, Y. Lee, J. Lee, T. H. Lee, J. Y. Park,; H. Seo, J. N. Lee, J. H. Oh, Y.-S. Choi, S. S. Lee, A centrifugally actuated point-of-care testing system for the surface acoustic wave immunosensing of cardiac troponin I, Analyst 138 (9) (2013) 2558-2566, https://doi.org/10.1039/C3AN00182B.

[22] G. Oudeng, M. Benz, A.A. Popova, Y. Zhang, C. Yi, P.A. Levkin, M. Yang, Droplet Microarray Based on Nanosensing Probe Patterns for Simultaneous Detection of Multiple HIV Retroviral Nucleic Acids, ACS Appl. Mater. Interfaces 12 (50) (2020) 55614–55623, https://doi.org/10.1021/acsami.0c16146.

[23] A.D. Chowdhury, K. Takemura, T.C. Li, T. Suzuki, E.Y. Park, Electrical pulse-induced electrochemical biosensor for hepatitis E virus detection, Nat. Commun. 10 (1) (2019) 3737, https://doi.org/10.1038/s41467-019-11644-5.

[24] D.K. Ban, T. Bodily, A.G. Karkisaval, Y. Dong, S. Natani, A. Ramanathan, A. Ramil, S. Srivastava, P. Bandaru, G. Glinsky, R. Lal, Rapid self-test of unprocessed viruses of SARS-CoV-2 and its variants in saliva by portable wireless graphene biosensor, Proc. Natl. Acad. Sci. U S A 119 (28) (2022), https://doi.org/10.1073/pnas.220652111.

[25] R. Wang, R. Zhao, Y. Li, W. Kong, X. Guo, Y. Yang, F. Wu, W. Liu, H. Song, R. Hao, Rapid detection of multiple respiratory viruses based on microfluidic isothermal amplification and a real-time colorimetric method, Lab Chip 18 (22) (2018) 3507–3515, https://doi.org/10.1039/C8LC00841H.

[26] C. Escobedo, Y.W. Chou, M. Rahman, X. Duan, R. Gordon, D. Sinton, A.G. Brolo, J. Ferreira, Quantification of ovarian cancer markers with integrated microfluidic concentration gradient and imaging nanohole surface plasmon resonance, Analyst 138 (5) (2013) 1450–1458, https://doi.org/10.1039/C3AN36616B.

[27] Z. Zhang, P. Ma, R. Ahmed, J. Wang, D. Akin, F. Soto, B.F. Liu, P. Li, U. Demirci, Advanced Point-of-Care Testing Technologies for Human Acute Respiratory Virus Detection, Adv. Mater. 34 (1) (2022) e2103646.

[28] B. Giri, S. Pandey, R. Shrestha, K. Pokharel, F.S. Ligler, B.B. Neupane, Review of analytical performance of COVID-19 detection methods, Anal. Bioanal. Chem. 413 (1) (2021) 35–48, https://doi.org/10.1007/s00216-020-02889-x.

[29] S.R. Dash, C.N. Kundu, Advances in nanomedicine for the treatment of infectious diseases caused by viruses, Biomater. Sci. 11 (10) (2023) 3431–3449, https://doi.org/10.1039/D2BM02066A.

[30] A.A. Yanik, M. Huang, O. Kamohara, A. Artar, T.W. Geisbert, J.H. Connor, H. Altug, An optofluidic nanoplasmonic biosensor for direct detection of live viruses from biological media, Nano Lett. 10 (12) (2010) 4962–4969, https://doi.org/10.1021/nl103025u.

[31] S.U. Son, S.B. Seo, S. Jang, J. Choi, J.-W. Lim, D.K. Lee, H. Kim, S. Seo, T. Kang, J. Jung, E.-K. Lim, Naked-eye detection of pandemic influenza a (pH1N1) virus by polydiacetylene (PDA)-based paper sensor as a point-of-care diagnostic platform, Sens. Actuators B 291 (2019) 257–265, https://doi.org/10.1016/j.snb.2019.04.081.

[32] G.L. Liu, Y. Yin, S. Kunchakarra, B. Mukherjee, D. Gerion, S.D. Jett, D.G. Bear, J. W. Gray, A.P. Alivisatos, L.P. Lee, F.F. Chen, A nanoplasmonic molecular ruler for measuring nuclease activity and DNA footprinting, Nat. Nanotechnol. 1 (1) (2006) 47–52, https://doi.org/10.1038/nnano.2006.51.

[33] R. Wang, L. Xu, Y. Li, Bio-nanogate controlled enzymatic reaction for virus sensing, Biosens. Bioelectron 67 (2015) 400–407, https://doi.org/10.1016/j.bios.2014.08.071.

[34] A.S. Peinetti, R.J. Lake, W. Cong, L. Cooper, Y. Wu, Y. Ma, G.T. Pawel, M.E. Toimil-Molares, C. Trautmann, L. Rong, B. Mariñas, O. Azzaroni, Y. Lu, Direct detection of human adenovirus or SARS-CoV-2 with ability to inform infectivity using DNA aptamer-nanopore sensors, Sci. Adv. 7 (39) (2021) eabh2848, https://doi.org/10.1126/sciadv.abh284.

[35] H. Yousefi, A. Mahmud, D. Chang, J. Das, S. Gomis, J.B. Chen, H. Wang, T. Been, L. Yip, E. Coomes, Z. Li, S. Mubareka, A. McGeer, N. Christie, S. Gray-Owen, A. Cochrane, J.M. Rini, E.H. Sargent, S.O. Kelley, Detection of SARS-CoV-2 Viral Particles Using Direct, Reagent-Free Electrochemical Sensing, J. Am. Chem. Soc. 143 (4) (2021) 1722–1727, https://doi.org/10.1021/jacs.0c10810.

[36] P.Q. Nguyen, L.R. Soenksen, N.M. Donghia, N.M. Angenent-Mari, H. de Puig, A. Huang, R. Lee, S. Slomovic, T. Galbersanini, G. Lansberry, H.M. Sallum, E. M. Zhao, J.B. Niemi, J.J. Collins, Wearable materials with embedded synthetic biology sensors for biomolecule detection, Nat. Biotechnol. 39 (11) (2021) 1366–1374, https://doi.org/10.1038/s41587-021-00950-3.
[37] X. Qian, B. Städler, Polydiacetylene-Based Biosensors for the Detection of Viruses and Related Biomolecules, Adv. Funct. Mater. 30 (49) (2020) 2004605, https://doi.org/10.1002/adfm.202004605.
[38] A. Dahlin, M. Zach, T. Rindzevicius, M. Kall, D.S. Sutherland, F. Hook, Localized surface plasmon resonance sensing of lipid-membrane-mediated biorecognition events, J. Am. Chem. Soc. 127 (14) (2005) 5043–5048, https://doi.org/10.1021/ja043672o.
[39] J.A. Jackman, E. Linardy, D. Yoo, J. Seo, W.B. Ng, D.J. Klemme, N.J. Wittenberg, S. H. Oh, N.J. Cho, Plasmonic Nanohole Sensor for Capturing Single Virus-Like Particles toward Virucidal Drug Evaluation, Small 12 (9) (2016) 1159–1166, https://doi.org/10.1002/smll.201501914.
[40] E.N. Özmen, E. Kartal, M.B. Turan, A. Yazıcıoğlu, J.H. Niazi, A. Qureshi, Graphene and carbon nanotubes interfaced electrochemical nanobiosensors for the detection of SARS-CoV-2 (COVID-19) and other respiratory viral infections: a review, Mater. Sci. Eng. C 129 (2021) 112356, https://doi.org/10.1016/j.msec.2021.112356.
[41] Z.-J. Zhao, S.H. Hwang, S. Jeon, J.-Y. Jung, J. Lee, D.-G. Choi, J.-H. Choi, S.-H. Park, J.-H. Jeong, Effects of polymer surface energy on morphology and properties of silver nanowire fabricated via nanoimprint and E-beam evaporation, Appl. Surf. Sci. 420 (31) (2017) 429–438, https://doi.org/10.1016/j.apsusc.2017.05.184.
[42] S.J. Pearton, D.P. Norton, Dry Etching of Electronic Oxides, Polymers, and Semiconductors, Plasma Process. Polym. 2 (2005) 16–37, https://doi.org/10.1002/ppap.200400035.
[43] R. C. MacDonald, R. I. MacDonald, B. Ph. M. Menco, K. Takeshita, N. K. Subbarao, L. Hu, Small-Volume extrusion apparatus for preparation of large, unilamellar vesicles, Biochimica et Biophysica Acta (BBA) - Biomembranes 1061 (2) (1991) 297-303, https://doi.org/10.1016/0005-2736(91)90295-J.
[44] B.J. Berne, R. Pecora, Dynamic light scattering: with applications to chemistry, biology, and physics, Courier Corporation (2000).
[45] M. Yuce, E. Filiztekin, K.G. Ozkaya, COVID-19 diagnosis -A review of current methods, Biosens. Bioelectron. 172 (2021) 112752, https://doi.org/10.1016/j.bios.2020.112752.
[46] G. Giovannini, H. Haick, D. Garoli, Detecting COVID-19 from Breath: A Game Changer for a BigChallenge, ACS Sensors 6 (2021) 1408–1417. https://pubs.acs.org/doi/full/10.1021/acssensors.1c00312.
[47] Z.J. Zhao, S.H. Shin, S.Y. Lee, B. Son, Y. Liao, S. Hwang, S. Jeon, H. Kang, M. Kim, J.H. Jeong, Direct chemisorption-assisted nanotransfer printing with wafer-scale uniformity and controllability, ACS Nano 16 (1) (2022) 378–385, https://doi.org/10.1021/acsnano.1c06781.
[48] J.A. Jackman, A.R. Ferhan, N.-J. Cho, Nanoplasmonic sensors for biointerfacial science, Chem. Soc. Rev. 46 (2017) 3615–3660, https://doi.org/10.1039/C6CS00494F.
[49] B.K. Yoon, W.-Y. Jeon, T.N. Sut, N.-J. Cho, J.A. Jackman, Stopping membrane-enveloped viruses with nanotechnology strategies: Toward antiviral drug development and pandemic preparedness, ACS Nano 15 (1) (2020) 125–148, https://doi.org/10.1021/acsnano.0c07489.
[50] J. Li, J. Ye, C. Chen, Y. Li, N. Verellen, V.V. Moshchalkov, L. Lagae, P. Van Dorpe, Revisiting the Surface Sensitivity of Nanoplasmonic Biosensors, ACS Photonics 2 (3) (2015) 425–431, https://doi.org/10.1021/ph5004779.
[51] F. Mazzotta, T.W. Johnson, A.B. Dahlin, J. Shaver, S.-H. Oh, F. Höök, Influence of the Evanescent Field Decay Length on the Sensitivity of Plasmonic Nanodisks and Nanoholes, ACS Photonics 2 (2) (2015) 256–262, https://doi.org/10.1021/ph500360d.
[52] M. Najiminaini, F. Vasefi, B. Kaminska, J.J.L. Carson, Nano-hole array structure with improved surface plasmon energy matching characteristics, Appl. Phys. Lett. 100 (2012) 043105, https://doi.org/10.1063/1.3679173.